de Chaunac, H. & Holeyman, A. (2018). *Géotechnique* **68**, No. 4, 332–344 [https://doi.org/10.1680/jgeot.16.P.229]

Numerical analysis of the set-up around the shaft of a closed-ended pile driven in clay

H. DE CHAUNAC* and A. HOLEYMAN*

When a pile is driven into the ground, soil standing in the path of the pile is heavily distorted as it has to cede for the penetrating pile. At the end of installation, this soil is left in a distressed state, which progressively evolves to an equilibrium with time. As a result, for lightly overconsolidated clays, soil resistance generally decreases during driving but increases after installation; the latter phenomenon is referred to as set-up. Correct assessment of pile set-up is one of the most important considerations of displacement pile design, especially offshore. Indeed, underestimation of set-up leads to unnecessary expense and overestimation of set-up leads to a precarious overestimation of the pile capacity. This paper presents a numerical model, the aim of which is to predict set-up around the shaft of a driven pile in clay. The model was conceived after a careful literature review of the relevant field data, in order to support its assumptions. It is used to predict the stress and pore pressure distributions around the shaft of a driven pile during installation and subsequent equalisation. Numerical results are then compared to the literature results. Although the model underestimates the excess pore pressure created around the pile, it captures a key feature of displacement pile installation in clay: at the end of installation, the radial distribution of excess pore pressure presents a peak located a few radii away from the pile wall. This implies that, during equalisation, the radial effective stress at the pile wall decreases to a short-term minimum, leading to a short-term minimum in pile capacity, before eventually increasing.

KEYWORDS: clays; consolidation; numerical modelling; piles & piling; pore pressures

INTRODUCTION

Pile driving is the oldest, the simplest and the most popular pile installation method, with over 40% of all piles installed worldwide being driven piles (Bottiau, 2006). Driven piles exhibit a peculiar characteristic shared by all displacement piles: their static capacity evolves with time after installation. Once a pile has been driven to its desired embedment, the soil surrounding the pile is left in a distressed state. Over time, the soil evolves to an equilibrium, leading to a change in pile capacity. This phenomenon is referred to as either 'set-up' when pile capacity increases during equalisation or 'relaxation' when the pile capacity decreases.

In soft, clayey soils, the pile capacity usually rises during equalisation, where the pile capacity can increase up to six-fold with regard to the end of driving capacity (Poulos, 1988; Rausche *et al.*, 2004).

Soil set-up is one of the most important considerations in planning a successful pile installation, especially offshore (Vijayvergiya *et al.*, 1977). Underestimation of soil set-up might result in unforeseen pile driving refusal after a driving interruption or might lead the installation engineer to erroneously drive the pile deeper than its design penetration. Both cases of ill judgement would result in additional expensive operations, such as replacing the hammer for the former and mobilisation of supplementary pile materials for the latter. Conversely, overestimation of soil set-up would be an even greater peril, as the pile capacity would never reach its design value.

Manuscript received 30 August 2016; revised manuscript accepted 22 June 2017. Published online ahead of print 23 August 2017. Discussion on this paper closes on 1 September 2018, for further details see p. ii.

* Department of Civil and Environmental Engineering, Université catholique de Louvain, Louvain-la-Neuve, Belgium.

The objective of the work presented in this paper was to implement a numerical method able to predict soil set-up or relaxation around the shaft of a driven pile in clay. In order to arrive at some meaningful results, the development of a numerical tool was preceded by a literature review of field, laboratory and numerical models of pile installations in clay. This is summarised in the next section of this paper, entitled 'Background'. The following two sections present the critical state-based constitutive relationship used to replicate the stress–strain behaviour of clay and the numerical tools developed to model the pile installation and equalisation stages. Next, the numerical model results are presented and compared with relevant field data.

BACKGROUND

During installation, the soil in close vicinity to the pile is heavily deformed as it has to accommodate the penetrating pile. Over most of the pile depth, this soil is kinematically constrained by the pile wall rigid boundary and the overburden stress of the overlying soil. Therefore, installation heavily changes both the total stress and the pore pressure of the soil close to the pile. When the pile has attained its desired embedment, the excess pore pressure slowly tends to equalise and the effective stress changes accordingly. In clay, the variation of pile capacity during equalisation occurs as a result of pore pressure dissipation around the pile (Randolph, 2003). Although set-up is also observed in sand or chalk (Vijayvergiya *et al.*, 1977; Jardine *et al.*, 2006), the presented work focuses solely on clay soils.

In order to rationalise and predict set-up, a number of studies have been performed during the last 50 years, either using model piles or numerical simulations. The next two subsections give a condensed literature review of each of these categories – the comprehensive version of this literature review can be found in de Chaunac (2015).

Model test of pile installation

Driven by the offshore industry, research involving model pile installations in clay peaked at the end of the last century. Typical research comprises a model pile jacked in clay, either in a laboratory or in the field. The quantities measured during such an experiment are pore pressure, radial total stress and shear stress on the pile wall (e.g. Soares & Dias, 1989), sometimes supplemented by pore pressure measurements in the surrounding soil (e.g. Roy *et al.*, 1981).

The literature reviewed by the authors comprised 62 model pile installations in 12 field locations from seven research groups. The average soil conditions, pile characteristics and references of the investigated literature are described in Table 1.

The main conclusions are listed below.

(*a*) In clays, soil strength variations during driving and subsequent equalisation are mainly governed by the variation of excess pore water pressure (Δu) around the pile (Randolph & Gourvenec, 2011).

(*b*) As the pile penetrates into the ground, the stress and pore pressure around the pile vary with h, the vertical distance from the pile toe (Karlsrud & Haugen, 1985; Coop, 1987; Konrad & Roy, 1987; Bond & Jardine, 1991). This phenomenon is named the h/R effect (Bond & Jardine, 1991) and has two causes: (i) a particular soil horizon unloads vertically when the pile toe passes that level (Fig. 1(a)) and (ii) the cycles of shaft–soil shearing induce cyclic adaptation of the soil adjacent to the pile wall (Fig. 1(b); Heerema, 1980).

(*c*) The radial total stress (σ_r) consistently decreases with vertical distance (h), whatever the initial overconsolidation ratio (Karlsrud & Haugen, 1985; Coop & Wroth, 1989; Soares & Dias, 1989; Bond & Jardine, 1991; Lehane & Jardine, 1994a, 1994b). The radial effective stress (σ'_r) depicts similar behaviour (Azzouz & Lutz, 1986; Coop & Wroth, 1989; Lehane & Jardine, 1994a, 1994b). However, the excess pore pressure sometimes increases with vertical distance from the pile toe (h) (Coop & Wroth, 1989; Lehane & Jardine, 1994b), although the more general trend is a decrease with increasing h (Konrad & Roy, 1987; Soares & Dias, 1989; Bond & Jardine, 1991).

(*d*) The strength variation during driving is a manifestation of the h/R effect (Jardine *et al.*, 2005).

(*e*) At the end of installation, the radial effective stress (σ'_{ri}) is lower than the overburden radial effective stress (σ'_{r0}) for lightly consolidated clays (Azzouz & Lutz, 1986; Lehane & Jardine, 1994a) but higher than σ'_{r0} for overconsolidated clays (Bond & Jardine, 1991; Lehane & Jardine, 1994b).

(*f*) The pore pressure changes that occur during equalisation take place alongside a decrease in total radial stress (σ_r), which induces a change in the radial effective stress (σ'_r) acting on the pile wall (e.g. Azzouz & Morrison, 1988; Lehane & Jardine, 1994a, 1994b). The latter governs the static unit skin friction (τ_f) through a Coulomb-type friction law (Jardine *et al.*, 2005).

(*g*) Most of the reviewed field data, as well as the numerical simulations presented in this paper, focus on the shaft of the pile. Therefore, a set-up factor can be expressed in terms of unit skin friction resistance which, as pointed out above, increases with the radial effective stress. The following definition can therefore be conveniently used, as an indicator of the actual set-up or relaxation the soil has encountered

$$\text{Radial effective stress set-up factor} = \frac{\sigma'_{rc}}{\sigma'_{ri}} \tag{1}$$

where σ'_{rc} and σ'_{ri} are the radial effective stresses after equalisation and after installation, respectively.

(*h*) During equalisation, a short-term increase in excess pore pressure (Δu) is consistently observed at the pile wall during the first minutes of equalisation, regardless of the initial overconsolidation ratio (Steenfelt *et al.*, 1981; Coop & Wroth, 1989; Soares & Dias, 1989; Bond & Jardine, 1991; Lehane & Jardine, 1994a, 1994b). This leads to a decrease in radial effective stress around the shaft and therefore to a decrease in pile capacity during the first minutes of equalisation (Azzouz & Lutz, 1986; Azzouz & Morrison, 1988; Coop & Wroth, 1989; Lehane & Jardine, 1994a, 1994b).

(*i*) This short-term increase in Δu appears to be confined to a narrow zone around the pile, since pore pressure transducers installed in the soil show no corresponding effect (Roy *et al.*, 1981; Pestana *et al.*, 2002), even for measurements made at 0·5 radii from the pile shaft (Steenfelt *et al.*, 1981).

(*j*) At the end of equalisation, the radial effective stress (σ'_{rc}) is higher or equal to the overburden radial stress (σ'_{r0}) whatever the initial overconsolidation ratio (Karlsrud & Haugen, 1985; Azzouz & Lutz, 1986; Azzouz & Morrison, 1988; Bond & Jardine, 1991; Lehane & Jardine, 1994a, 1994b). However, the radial effective stress set-up factor (equation (1)) is larger than or equal to one for lightly overconsolidated clays (Azzouz & Lutz, 1986; Lehane & Jardine, 1994a), but smaller than one for heavily overconsolidated clays (Bond & Jardine, 1991; Lehane & Jardine, 1994b).

Table 1. Representative average soil conditions and pile types of the field data investigated

Clay					Model pile			Reference
Name	OCR	PI	LI	S_t	D: mm	L_{max}: m	No. tests	
London	30·0	45	0·0	1	102	6·2	4	Bond & Jardine (1991)
Bothkennar	1·7	40	0·7	5	102	6	4	Lehane & Jardine (1994a)
Cowden	10·0	19	−0·2	1	102	6·4	4	Lehane & Jardine (1994b)
Pentre	2·0	15	0·5	2	102	19	7	Chow (1996)
Empire	1·7	60	0·3	2	38·4	77	2	Azzouz & Lutz (1986)
Boston Blue	1·2	21	1·0	7	38·4	39	6	Azzouz & Morrison (1988)
Rio	1·8	60	1·6	NA	220	7	1	Soares & Dias (1989)
London	30·0	45	0·0	1	80	5	1	Coop (1987)
Gault	10	48	0·0	NA	80	8	6	Coop & Wroth (1989)
Huntspill	1·6	35	1·0	NA	80	9	2	Coop & Wroth (1989)
Haga	5·0	15	1·0	5	153	5	17	Karlsrud & Haugen (1985)
Champlain	2·2	15	2·3	17	219	7·6	7	Roy *et al.* (1981) and Konrad & Roy (1987)
Young Bay	1·3	40	0·9	NA	610	36	1	Pestana *et al.* (2002)

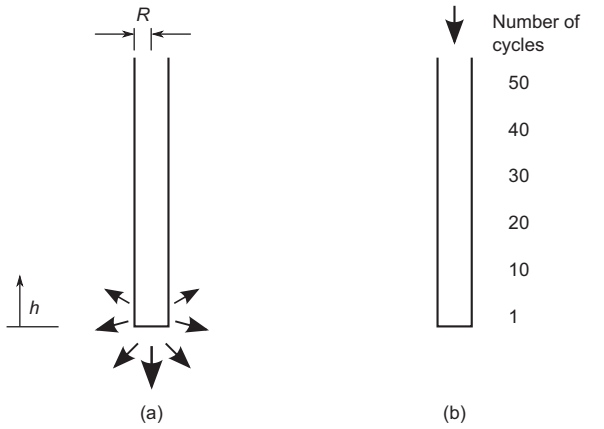

Fig. 1. Possible reasons for the *h*/*R* effect during deep penetration (after Chow, 1996): (a) relative location of the region of high stresses around the pile toe; (b) number of shearing cycles encountered by the soil horizon

Numerical simulation of pile installation

Since the second half of the twentieth century, a limited number of rational approaches have emerged to model the installation process. The next four paragraphs summarise the numerical methods used to simulate pile installation and the fifth paragraph describes the numerical tools available to model the equalisation stage.

The cavity expansion method is the oldest rational approach to model pile installation. Notable analytical solutions include Soderberg (1962), Butterfield & Bannerjee (1970), Vesić (1972) or Randolph & Wroth (1979). The cavity expansion method produces straightforward results and closely replicates the radial displacement field around the shaft of a displacement pile (Randolph *et al.*, 1979; Steenfelt *et al.*, 1981; Pestana *et al.*, 2002; Lehane & Gill, 2004). However, it neither accounts for the complex strain paths followed by the soil near the pile toe nor for the repeated shaft–soil shearing cycles inducing cyclic adaptation of the soil.

Introduced by Baligh (1985), the strain path method brought the next leap in rational approaches to model pile installation. The strain path method is an analytical framework that sees the penetration process as a steady flow of incompressible soil past a stationary pile, formed by a spherical source emitting an incompressible material at a constant rate. The strain path method hinges on the assumption that soil deformations during deep penetration can be estimated with a reasonable degree of accuracy without the need to consider a constitutive relationship for the soil. This assumption leads to a violation of either the equilibrium equations or the constitutive relationship. The main enhancement offered by the strain path method is that it captures the dependence of the deformations on the vertical coordinate: as the pile descends into the ground, the soil particles undergo vertical and radial movement. However, the method does not take into account the cycles of shaft–soil shearing during installation. Some notable enhancements involving the strain path method include Chin (1986), who used a ring source to perform an open-ended pile installation, and Sagaseta *et al.* (1997), who accounted for soil surface movement.

In the last 20 years, the finite-element method has emerged due to the increase in available computing power. Three main approaches are used: the arbitrary Lagrangian–Eulerian method (ALE; e.g. Jassim *et al.*, 2013; Sabetamal *et al.*, 2014); the coupled Eulerian–Lagrangian method (CEL; e.g. Andresen & Khoa, 2013; Hamann *et al.*, 2015); and the remeshing and interpolation technique with small strain method (RITSS; e.g. Tian *et al*, 2014). The finite-element method is potentially the most accurate numerical tool as it can account for the pile geometry, inertia effects, cycles, equilibrium and advanced constitutive relationships. However, finite-element methods are cumbersome, time consuming and very complex to implement.

Alongside the three aforementioned approaches have emerged a number of 'alternative' methods. They are cruder but simpler than the large-strain finite-element methods. Two of these are outlined in this paragraph. Su (2010) approximates the strain field around an advancing cone in six zones, each of which is subjected to a simple mode of deformation, such as spherical cavity expansion, cylindrical cavity expansion, or plane strain shearing. Basu *et al.* (2013) separate the installation into two stages: cavity expansion, which represents the insertion of the pile toe, followed by a series of quasi-static shearing cycles, which represent the jacking cycles.

The equalisation stage, in clay soils, is mainly controlled by the consolidation, during which the dissipation of excess pore pressure leads to a variation in effective stress around the pile. The theory of consolidation has reached a stage where there is a general consensus on the governing equations (Coussy, 2004). The results of the consolidation analysis depend mainly on three factors: the soil conditions at the start of the analysis, the choice of coupled or uncoupled consolidation and the constitutive model.

The literature review led to the conclusion that to strive for a realistic and innovative simulation of the pile driving and equalisation stages, the following aspects should be accounted for. The installation simulation should include strain reversal around the pile toe, stress relaxation as the soil passes above the pile toe (one aspect of the *h*/*R* effect, Fig. 1(a)) and cyclic loading of the soil around the shaft (the other aspect of the *h*/*R* effect, Fig. 1(b)). The equalisation simulation should be coupled to account for the total stress decrease during equalisation. Finally, the constitutive model should be able to tackle overconsolidation ratio (OCR), high strains, cyclic loading and shear-induced pore pressures.

Before presenting the numerical model developed to simulate installation and equalisation, the following section introduces the constitutive model used.

CONSTITUTIVE MODEL

This section presents the constitutive model used to predict the clay stress–strain response, which is eventually used in the pile driving and equalisation models described in the following section.

The selected constitutive model is hypoplasticity for clay (Mašín, 2005) coupled to the intergranular strain concept (Niemunis & Herle, 1997). The former is aimed at reproducing the effective stress behaviour of clays in three dimensions during one loading–unloading cycle, while the latter accounts for small-strain stiffness degradation and strain reversals. There are ten material parameters, defined in Table 2 for London Clay.

Following Butterfield (1979), the volumetric behaviour of the hypoplastic model is defined in the ln v–ln p' plane instead of the v–ln p' plane. Isotropic loading from an isotropically normally consolidated state follows a straight line – the isotropic normal compression line – in the ln v–ln p' plane, but unloading follows a curve. Therefore, overconsolidation ratio is defined as

$$\mathrm{OCR}^* = \frac{p'_{\mathrm{e}}}{p'} \tag{2}$$

Table 2. London Clay parameters (adapted from Mašín, 2005)

Clay hypoplasticity					Intergranular strain				
ϕ'_{cs}	λ^*	κ^*	N^*	r^*	m_R	m_T	R^*	β_r	χ
22·6°	0·11	0·016	3·96	0·4	4	2	10^{-4}	0·2	1

Note: Parameter N^* is used instead of $N = \ln N^*$ defined in Mašín (2005).

where p' is the current mean effective stress and p'_e is the constant volume projection of the current mean effective stress on the isotropic normal compression line (also named Hvorslev's equivalent pressure). Since equation (2) differs from the conventional definition of overconsolidation ratio, Appendix 1 provides a relationship between the two definitions.

The constitutive model is by definition a simplification of the reality. It does not account for several features of clayey soils, such as rate dependence, anisotropy, residual state, or structure. However, the constitutive model has the following desirable features for the simulation of pile driving: (*a*) it follows the conceptual framework of critical state soil mechanics (Schofield & Wroth, 1968); (*b*) it uses a small number of material parameters that can be determined from standard laboratory tests (Mašín, 2012); (*c*) it predicts stiffness degradation with strain; (*d*) it takes into account cyclic loading by modelling the stiffness increase as the loading direction changes; (*e*) it models shear-induced dilatancy; and (*f*) it is straightforward to implement.

An example illustrating the capabilities of the hypoplastic model for clays, including intergranular strain features, is provided in Appendix 2.

INSTALLATION AND EQUALISATION MODEL

This section presents the numerical analysis used to model pile installation and equalisation, which both make use of the hypoplastic constitutive relationship presented in the previous section.

Two main assumptions lay behind the concept of the numerical model developed in this paper. First of all, in saturated clay, the briskness of pile driving coupled to the low permeability of clays imply that pile installation can be considered to be an undrained process. Furthermore, it can be reasonably assumed that soil not too close to the surface or to the pile toe is kinematically constrained in plane strain conditions. Therefore, instead of modelling the entire pile, the present analysis focuses on a thin plane strain disc of clay around a driven pile during and after installation, following a radial model suggested by Holeyman (1985) (Fig. 2).

Installation

Pile installation modelling is split into two steps. The first step creates the straining history of each soil particle of the disc of clay due to the insertion of the pile toe (Fig. 3(a)). The second step subjects this disc of clay to a series of shearing events, aiming to reproduce the shaft–soil shearing occurring during pile driving (Fig. 3(b)).

The first step makes use of the strain path method, an approximate analytical framework introduced by Baligh (1985), which models the steady penetration of a pile into the ground. The strain path method consists of a spherical cavity emitting an incompressible material (the pile) at a volume rate of V per unit of time, embedded in a uniform flow field (the soil) with velocity U in the z direction. The soil is considered incompressible, the geometry axisymmetric and the flow irrotational. The soil radial and vertical velocity components of each soil particle (v_r and v_z, respectively) are therefore explicitly defined

$$v_r = \frac{1}{r}\frac{\partial \Psi}{\partial z} \tag{3}$$

$$v_z = \frac{-1}{r}\frac{\partial \Psi}{\partial r} \tag{4}$$

where Ψ is a stream function

$$\Psi = \frac{V}{4\pi}\frac{z}{\sqrt{r^2 + z^2}} - \frac{r^2}{2}U \tag{5}$$

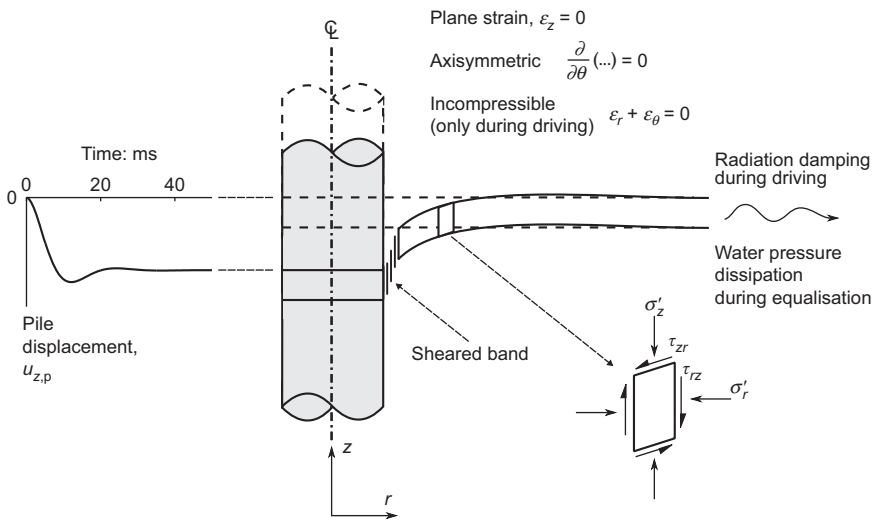

Fig. 2. Features of a disc of plane strain clay soil around a driven pile (after Holeyman, 1985)

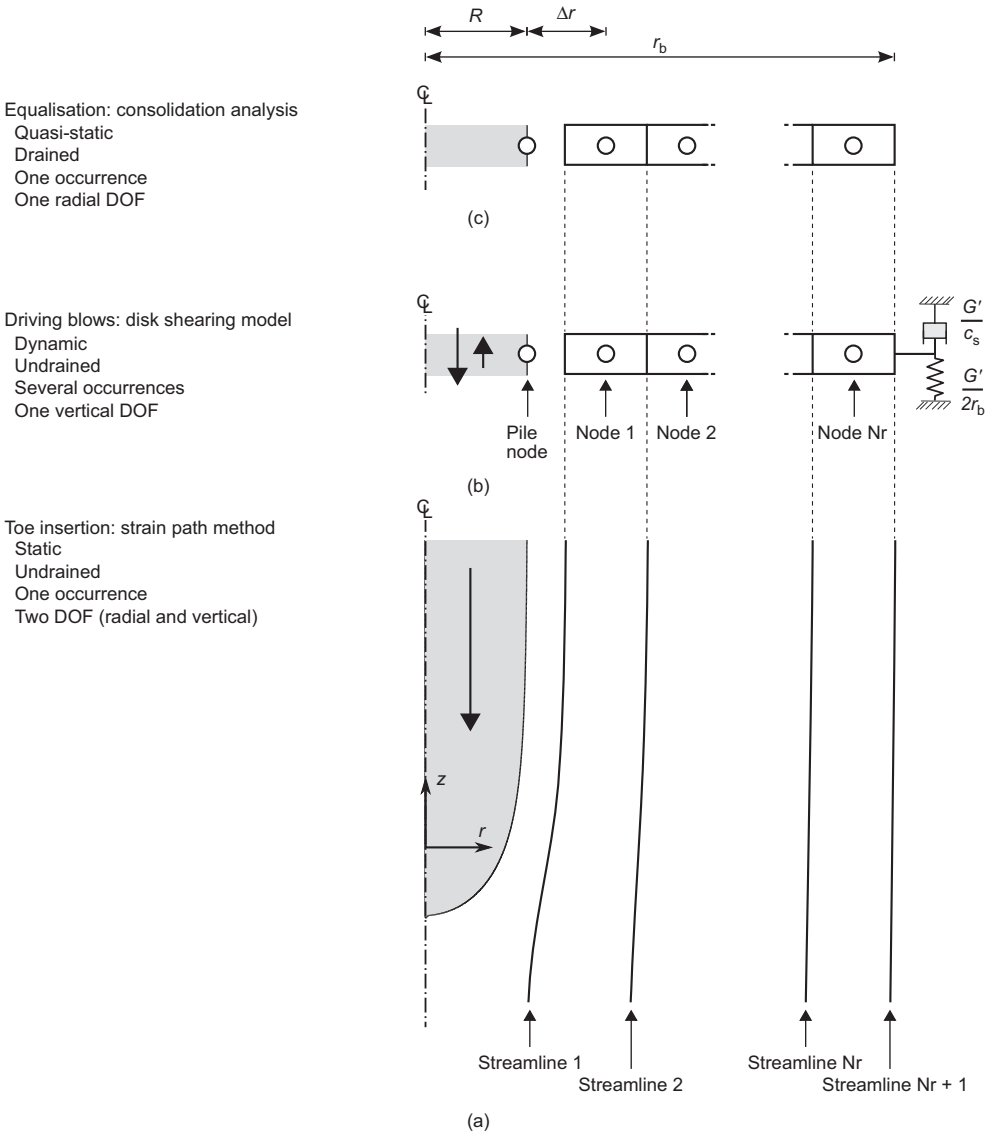

Fig. 3. Study of a disc of soil around a closed-ended driven pile: (a) and (b) simulate the installation stage and (c) simulates the equalisation stage

Continuity and incompressibility impose that V and U are related

$$\pi U R^2 = V \tag{6}$$

where R is the pile radius.

Starting from a layer of soil subjected to a geostatic overburden pressure (far below the pile toe, Fig. 3(a)), the equations (3) and (4) predict the streamlines followed by each of the soil particles investigated.

Far above the pile toe (typically, a distance of $10R$ above the pile toe), the soil state predicted by the strain path method is plane strain and independent of the distance from the pile toe. This soil state is taken as the initial condition for the disc shearing model, which imposes a series of driving blows on a thin plane strain disc of clay (Fig. 3(b)).

The disc shearing model uses an explicit dynamic one-dimensional Eulerian finite-difference scheme suggested by Holeyman (1985) and further developed by Vanden Berghe & Holeyman (2002). The disc shearing model discretises a plane strain layer of pile and soil as $\mathrm{Nr}+1$ nodes, the first one being the pile wall, and the other Nr nodes representing the soil (Fig. 3(b)). Kinematic quantities (displacement, velocity and acceleration) are evaluated at the nodes while stress, strain and void ratio are evaluated between the nodes. Soil is considered undrained and the hypoplastic constitutive model presented in the previous section is used.

The integration scheme of the disc shearing model is as follows. At each time step, strain rates between the nodes are computed from the node vertical velocities (v_z), all other velocities being null. Strain rates are converted to effective stresses by the constitutive model. Then, vertical acceleration at each pile node (a_z) is computed by integrating the vertical equation of motion

$$\frac{1}{r}\frac{\partial}{\partial r}(r\tau_{rz}) = \rho a_z \tag{7}$$

where r is the radial position, τ_{rz} is the shear stress and $\rho = n\rho_w + (1-n)\rho_s$ is the soil density, with ρ_w and ρ_s being the densities of the fluid and solid phases, and n the water porosity. Finally, vertical acceleration (a_z) is time integrated to obtain velocity (v_z) at the next time step.

The inner boundary of the disc shearing model is a node symbolising the pile wall (Fig. 3(b)), where pile velocity ($v_{z,p}$) is imposed as the closed form of an under-damped mass–spring–dashpot system (Holeyman, 1984)

$$v_{z,p} = 2v_0 \frac{\alpha}{\beta} e^{-\alpha t} \sin(\beta t) \tag{8}$$

where v_0 is the hammer initial velocity, and α and β are defined below

$$\alpha = \frac{k}{2I} \quad \beta = \sqrt{\omega_n^2 - \alpha^2} \quad \omega_n = \sqrt{\frac{k}{M}} \tag{9}$$

where M, k and I are, respectively, the mass, the stiffness of the spring and the impedance of the dashpot.

The integration scheme of the disc shearing model being dynamic, an appropriate 'absorbing' boundary must be selected in order to prevent energy from an outgoing wave from being reflected by the boundary. The pile transient velocity and the non-linearity of the constitutive model force the use of a frequency independent (thus approximate) absorbing boundary, which consists of a dashpot placed in parallel to a spring (Fig. 3(b)). The dashpot coefficient is selected so that no energy is reflected from the boundary in an elastic medium (Lysmer & Kuhlemeyer, 1969)

$$\tau_{rz} = \frac{G'}{c_s} v_z \tag{10}$$

where G' is the soil effective stress shear modulus, c_s is the soil shear wave velocity and v_z is the soil vertical velocity. In addition, a linear spring is needed in order for the boundary to be in equilibrium even under residual stress. In the absence of this spring, the shear stresses will eventually become null over the whole domain, with all final displacements being equal to the pile shaft displacement (Loukidis *et al*., 2008). Following Deeks & Randolph (1994), the spring coefficient taken herein is

$$\tau_{rz} = \frac{G'}{2r_b} u_z \tag{11}$$

where r_b is the boundary radius and u_z is the soil vertical displacement.

During the entire process, the pore pressure is computed. The geometry of the disc shearing model implies that the vertical equation of motion (equation (7)) is satisfied without having to take into account total stress. Therefore, pore pressure is computed through the radial equilibrium

$$\frac{\partial \sigma'_r}{\partial r} + \frac{\partial u}{\partial r} + \frac{1}{r}(\sigma'_r - \sigma'_\theta) = 0 \tag{12}$$

which can be solved for the pore water pressure (u) as the effective stresses σ'_r and σ'_θ are known. The boundary conditions to equation (12) are an impermeable pile at the inner boundary and a constant pore pressure at the outer boundary.

An example of the disc shearing model output is presented in de Chaunac & Holeyman (2014).

Equalisation

At the end of installation, the undrained assumption is relaxed and radial drainage of the thin disc of soil is permitted (Fig. 3(c)). The equalisation stage is modelled by a coupled consolidation analysis, using the following assumptions: (*a*) two phases are occupying the soil, the porous soil skeleton and the pore water, according to the Biot theory; (*b*) the skeleton behaviour is governed by an effective stress constitutive law; (*c*) the water flows through the porous skeleton according to Darcy's law, while tortuosity and dynamic inertia are neglected; (*d*) the fluid flow is quasi-static; that is. inertial forces are disregarded; (*e*) the soil grains composing the soil skeleton are much less compressible than the two-phase soil; (*f*) the pore water is much less compressible than the two-phase soil; (*g*) the permeability is assumed to be constant.

By using these assumptions, the mass balance equation and Darcy's law boil down to the following expressions of the soil and water radial velocities (respectively, v_r and $v_{r,w}$)

$$v_r = \frac{k_r}{\gamma_w} \frac{\partial u}{\partial r} \tag{13}$$

$$v_{r,w} = \frac{n-1}{n} v_r \tag{14}$$

where k_r is the radial permeability of the soil, γ_w is the water unit weight, u is the pore pressure and n is the porosity.

RESULTS

This section offers an overview of the results of the numerical model presented in the previous section. Five initial overconsolidation ratios are investigated and the numerical results are compared to field experiments described in the 'Background' section.

The simulations are performed for London Clay using the hypoplastic model described earlier, the material parameters of which are reproduced in Table 2. Table 3 describes the five initial states which are investigated: all five have an initial void ratio (e_0) of 1 but varying initial stresses (σ'_{v0} and K_0) so that their hypoplastic overconsolidation ratio, OCR* (i.e. the overconsolidation ratio used by the hypoplastic model ($=p'_c/p'$)) ranges from 1·1 to 20 (which, using equation (20), equates to a conventional OCR ranging from 1·0 to 64·1).

The geometry of the problem is as follows: the pile radius (R) is 25 cm and the radial discretisation (Δr) is $0{\cdot}08R = 20$ mm. The outer boundary position (r_b) is located at $60R$ (except during the disc shearing model simulations for which the outer boundary is reduced to $16R$), and the vertical extent of the domain for the strain path method is $80R$ ($40R$ above and $40R$ below the pile toe). The strain path method soil flow velocity (U) is taken as 1 m/s while the volume insertion (V) is chosen according to equation (6). The imposed velocity at the boundary of the disc shearing model is given by equation (8) with $v_0 = -3$ m/s, $\omega_n = 300$ rad/s and $\alpha = 0{\cdot}5\omega_n$. The values chosen for ω_n and α correspond to various combinations of mass–spring–dashpot

Table 3. Numerical values of the simulations input and output at the pile wall

Initial state				After installation		During equalisation		After 95% equalisation	
σ'_{v0}: kPa	K_0	OCR*	OCR	σ'_{ri}: kPa	Δu_i: kPa	Δu_{max}: kPa	At t: h	σ'_{rc}: kPa	$\sigma'_{rc}/\sigma'_{ri}$
590	0·615	1·1	1·0	158·44	222·30	294·64	3	305·85	1·93
170	0·939	3	3·4	171·82	−6·21	109·90	20	121·25	0·70
90	1·143	5	7·1	181·60	−73·44	60·44	32	89·50	0·49
37	1·492	10	21·1	193·83	−132·65	20·04	76	56·70	0·28
15	1·947	20	64·1	201·79	−167·46	3·00	273	25·84	0·13

systems, ranging from, for example, a 4 ton mass, a spring stiffness of 9·12 MN/m and an impedance of 0·19 MNs/m to, for example, a 100 ton mass with a spring stiffness of 227·97 MN/m and an impedance of 4·77 MNs/m. For the equalisation stage, the radial permeability coefficient (k_r) is taken as 10^{-8} m/s (Hight *et al.*, 2003).

Installation

The strain path method is run once (Fig. 3(a)), after which the disc shearing model is run 100 times (simulating the effect of 100 driving blows around the shaft of the pile; Fig. 3(b)). After 100 blows, the state of the thin disc of soil reaches a relatively stable steady state (i.e. one more blow brings barely any change to the soil state). That state is therefore referred to as 'after installation' and denoted by the subscript 'i'. The numerical results of the installation stage are depicted in Figs 4–7 and numerical values of stress and pore pressure at the pile wall after installation are summarised in Table 3.

Figure 4 depicts the evolution of the excess pore pressure ratio ($\Delta u/\sigma'_{v0}$) after each cycle of shearing imposed by the disc shearing model for the first overconsolidation ratio investigated (OCR* = 1·1). The radial distribution of excess pore pressure (Fig. 4(a)) evolves after each shearing cycle: pore pressure at the pile wall decreases while the location of the pore pressure peak shifts away from the pile wall. Fig. 4(b) illustrates the decrease of excess pore pressure at the pile wall plotted against the blow count. Each blow imposes a cycle of straining which leads to a decrease in pore pressure at the pile wall. This cyclic adaptation phenomenon was found to be one of the two causes of the h/R effect (Fig. 1(b)). It is also of note that the first few blows move the soil state to the dry side of the critical state line which, as a consequence, implies that the soil at the pile wall behaves as an overconsolidated clay. This can be seen in Fig. 4(b) where, after a few blows, the pore pressure during the blow is always less than the end-of-blow value.

The numerical data depicted in Fig. 4(b) are corroborated in the literature: pore pressure at the pile wall was consistently lower during pile movement than when the pile was stationary, whatever the initial overconsolidation ratio (Boston Blue, London, Bothkennar and Cowden clays; Azzouz & Morrison, 1988; Bond & Jardine, 1991; Lehane & Jardine, 1994a, 1994b).

Figures 5(a) and 5(b) depict the excess pore pressure ratio ($\Delta u/\sigma'_{v0}$) distribution after the strain path method and after 100 blows of the disc shearing model simulations, respectively. For the sake of clarity, only the first four overconsolidation ratios investigated are shown. After the strain path method (Fig. 5(a)), $\Delta u/\sigma'_{v0}$ is monotonic for initial overconsolidation ratio values (OCR*) of 1·1, 3 and 5, with values at the pile wall slightly below 1. For the heavily overconsolidated soil (OCR* = 10), the excess pore pressure ratio is close to 0 at the pile wall and is negative up to a distance of four radii from the pile wall.

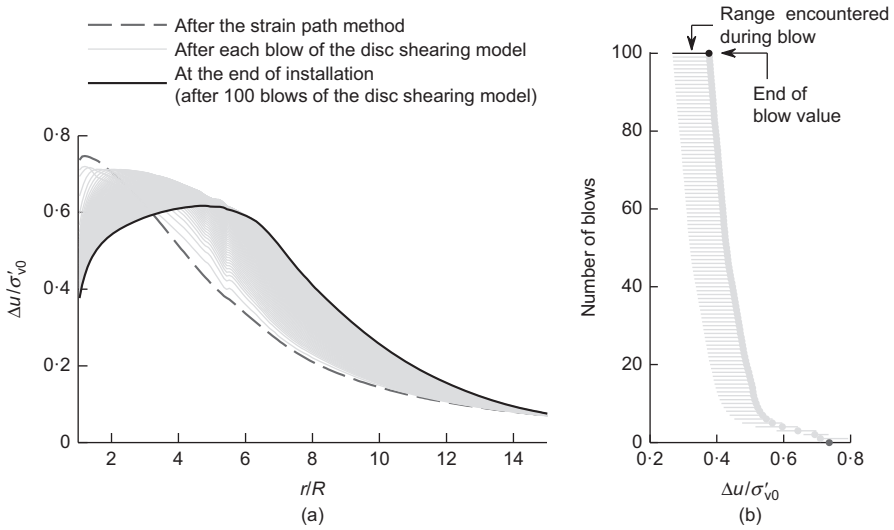

Fig. 4. Disc shearing model: pore pressure ratio after each driving blow for the OCR* = 1·1 initial state (a) over the domain and (b) at the pile wall

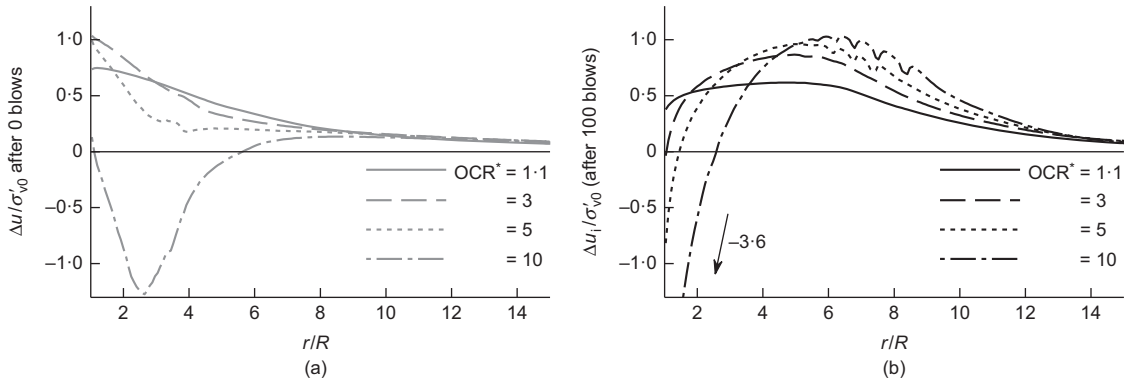

Fig. 5. Distribution of pore pressure (a) after the strain path method and (b) at the end of installation (after 100 blows of the disc shearing model)

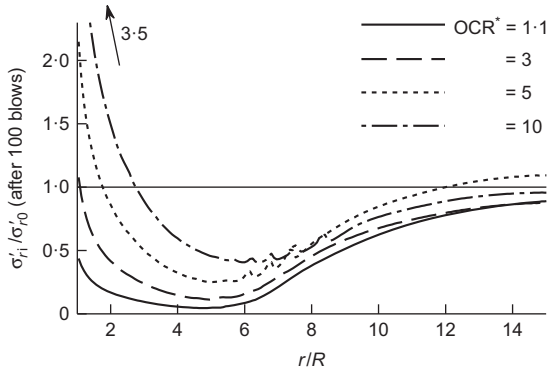

Fig. 6. Distribution of radial effective stress after installation

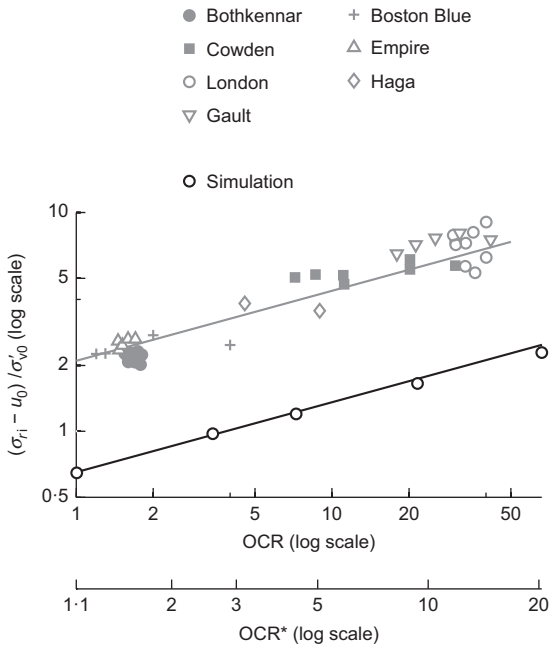

Fig. 7. Normalised radial total stress after installation plotted against overconsolidation ratio (hypoplastic OCR* and conventional OCR): experiments (jacked model piles, data compiled by Chow (1996)) and simulation

After 100 blows of the disc shearing model, the distribution of excess pore pressure ($\Delta u_i/\sigma'_{v0}$, denoted with a subscript 'i' for 'after installation') has drastically changed (Fig. 5(b)). The excess pore pressure ratio at the pile wall is now lower as the overconsolidation ratio is higher. The peak excess pore pressure ratio is located between three and six radii away from the pile wall and is higher as the overconsolidation ratio is higher. Each of the shaft–soil shearing cycles imposed by the disc shearing model has induced cyclic adaptation to the soil state around the pile (Fig. 1(b)).

Experimental data measured far above the pile toe evidenced the same trends as those reported in Fig. 5(b): at the pile wall, $\Delta u_i/\sigma'_{v0}$ was lower as overconsolidation ratio increased (Bothkennar clay, Cowden till and London Clay; Bond & Jardine, 1991; Lehane & Jardine, 1994a, 1994b), whereas $\Delta u_i/\sigma'_{v0}$ increased with overconsolidation ratio at radii exceeding $2R$ from the pile wall (Young Bay mud, Champlain clay and Haga clay; Roy *et al.*, 1981; Pestana *et al.*, 2002; Karlsrud, 2012). However, the simulated $\Delta u_i/\sigma'_{v0}$ is lower than the measured ratio: whereas $\Delta u_i/\sigma'_{v0}$ does not reach any higher values than 1 in the simulations, the experimental data suggest that the excess pore pressure ratio maximum attains values over 2, even for moderately overconsolidated soils.

The concave shape of simulated excess pore pressure after installation depicted in Fig. 5(b) stems from two aspects of the model: (*a*) the dynamic integration scheme of the disc shearing model takes into account soil inertia: each blow involves a cycle of strain and (*b*) the constitutive model handles shear-induced pore pressure variation due to loading cycles.

Figure 6 depicts the radial effective stress ratio after installation ($\sigma'_{ri}/\sigma'_{r0}$ – this time normalised to the initial radial effective stress for better comparison with the experimental data). At the pile wall, the radial effective stress after installation (σ'_{ri}) has decreased from its initial value (σ'_{r0}) for the lightly overconsolidated soil, whereas it has increased for the overconsolidated ones. For increasing radial position, the stress tends towards its initial value. However, all soils show a minimum σ'_{ri} between three and six radii away from the pile wall, corresponding to the peak Δu_i. The experimentally computed σ'_{ri} at the pile wall shared the same conclusions: $\sigma'_{ri} < \sigma'_{r0}$ for the lightly overconsolidated Bothkennar and Empire clays (Azzouz & Lutz, 1986; Lehane & Jardine, 1994a), whereas $\sigma'_{ri} > \sigma'_{r0}$ for the overconsolidated Cowden till and London Clay (Lehane & Jardine, 1994a).

The radial total stress ratio at the pile wall after installation (σ_{ri}/σ'_{v0}) is depicted in Fig. 7 plotted against overconsolidation ratio (hypoplastic OCR* and conventional OCR) and compared to experimental data. Simulated and experimental data concur concerning the positive gradient and the linear trend in a log–log plot. However, the measurements exceed the simulated data by at least a factor of 3.

EQUALISATION

Following the simulation of the installation stage (the strain path method and the 100 blows imposed by the disc shearing model), a coupled consolidation analysis is run to model the equalisation stage (Fig. 3(c)). The subscript '*c*' is used to denote equalised quantities, which are taken after 95% consolidation – that is, for a normalised pore pressure ratio ($\Delta u/\Delta u_{max}$) of 0·05 (Δu_{max} is the maximum pore pressure attained at the pile wall during equalisation). The simulation results are depicted in Figs 8–11 and numerical values attained at the pile wall during and after equalisation are summarised in Table 3.

The normalised pore pressure ratio at the pile wall ($\Delta u/\Delta u_{max}$) is depicted in Fig. 8 against dimensionless time (T) for the first four overconsolidation ratios investigated. Excess pore pressure initially increases to a maximum (Δu_{max}) before reducing. The origin of this initial

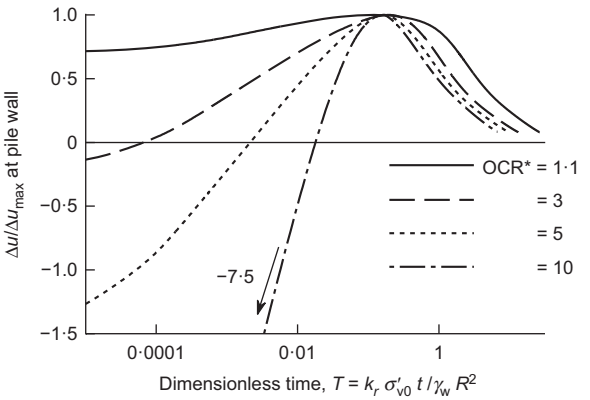

Fig. 8. Excess pore pressure ratio at the pile wall plotted against dimensionless time

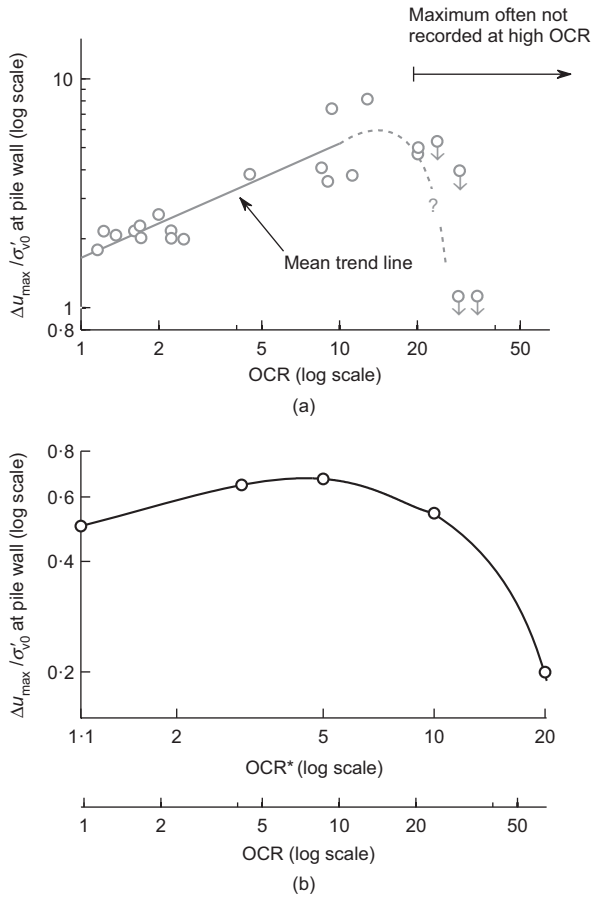

Fig. 9. Maximum pore pressure at the pile wall during equalisation plotted against overconsolidation ratios: (a) experiments (data compiled by Lehane (1992)) and (b) simulation

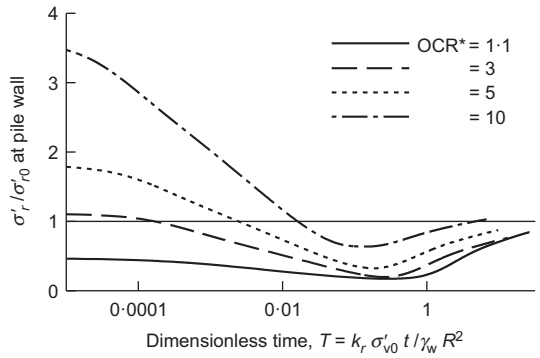

Fig. 10. Radial effective stress ratio at the pile wall plotted against dimensionless time

increase is the concave shape of the excess pore pressure distribution at the end of installation (Fig. 5(b)). As the maximum value of excess pore pressure lies a few radii away from pile shaft, the water initially flows towards the pile, leading to an increase in excess pore pressure (Δu). As a consequence of this short-term inward flow of water, not only does the effective stress decrease (this is discussed later) but the void ratio at the pile wall increases, which leads to a *drop* in shear strength (s_u). After the short-term increase, the pore pressure drops, following a classic consolidation pattern.

This short-term increase in pore pressure at the pile wall was consistently recorded in the field and laboratory studies, namely in kaolin, Rio de Janeiro, Gault, Hunspill, London and Bothkennar clays (Steenfelt *et al.*, 1981; Coop & Wroth, 1989; Soares & Dias, 1989; Bond & Jardine, 1991; Lehane & Jardine, 1994a, 1994b).

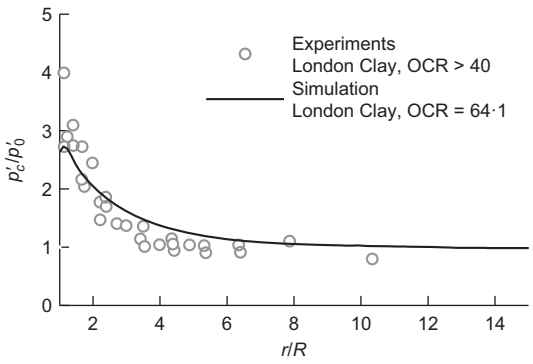

Fig. 11. Comparison between measured and simulated mean effective stress after installation and equalisation in London Clay (field data from Bond & Jardine (1991))

The value of the maximum excess pore pressure ratio ($\Delta u_{max}/\sigma'_{v0}$) recorded at the pile wall during this short-term rise against overconsolidation ratio is depicted in Fig. 9(a) for the field experiments. Up to an OCR of approximately 10, the ratio $\Delta u_{max}/\sigma'_{v0}$ rose with OCR. Above 10, $\Delta u_{max}/\sigma'_{v0}$ was often not recorded as pore pressure remained negative during most of the consolidation (Bond & Jardine, 1991). The numerical simulation results (Fig. 9(b)) depict a similar trend of increasing with overconsolidation ratio up to an OCR of around 10 before decreasing with OCR.

The reason for this trend can be inferred from the normalised excess pore pressure distribution ($\Delta u_i/\sigma'_{v0}$) at the end of installation (Fig. 5(b)). With increasing OCR, $\Delta u_i/\sigma'_{v0}$ at the pile wall reduces more strongly than the peak $\Delta u_i/\sigma'_{v0}$, located a few radii away from pile shaft, rises. Therefore, the increase in the peak Δu_i (located a few radii away from the pile wall) with OCR governs the increase of Δu_{max} until OCR ≈ 10. For higher values, Δu_{max} is governed by the negative Δu_i at the pile wall.

The radial effective stress ratio (σ'_r/σ'_{r0}) at the pile wall is depicted in Fig. 10 plotted against normalised time (T). The sharp short-term increase in pore water pressure (Fig. 8) leads to a rapid reduction in σ'_r. After that short-term decrease, σ'_r increases to values close to σ'_{r0}. The radial effective stress set-up factors ($\sigma'_{rc}/\sigma'_{ri}$) are summarised in Table 3. The radial effective stress set-up is greater than one for the normally consolidated soil ($\sigma'_{rc} > \sigma'_{ri}$) and is smaller than one for the overconsolidated soils.

Field experiments concur with the above-mentioned results. In Boston Blue, Empire, Gault, Hunspill, Cowden and Bothkennar clays, the radial effective stress on the pile shaft σ'_r showed a short-term drop followed by a long-term increase (Azzouz & Lutz, 1986; Azzouz & Morrison, 1988; Coop & Wroth, 1989; Lehane & Jardine, 1994a, 1994b). The radial effective stress set-up factor ($\sigma'_{rc}/\sigma'_{ri}$) was greater than one in lightly overconsolidated Empire clay (Azzouz & Lutz, 1986) and was equal to one in Bothkennar clay ($\sigma'_{rc} \approx \sigma'_{ri}$; Lehane & Jardine, 1994a). In the overconsolidated Cowden till and London Clay, the radial effective stress set-up factor was smaller than one (Bond & Jardine, 1991; Lehane & Jardine, 1994b).

Nevertheless, the simulations predict an equalised radial stress (σ'_{rc}) in the same range as σ'_{r0}, whereas the experiments report higher values: at the end of consolidation, the radial effective stress on the pile shaft (σ'_{rc}) was higher than the initial radial effective stress (σ'_{r0}) in overconsolidated soils (Cowden, London and Haga clays; Karlsrud & Haugen, 1985; Bond & Jardine, 1991; Lehane & Jardine, 1994b) and

normally consolidated soils (Bothekennar and Empire clays; Azzouz & Lutz, 1986; Lehane & Jardine, 1994a). Azzouz & Morrison (1988), in Boston Blue clay, found σ'_{rc} to be in the same range as σ'_{r0}.

Finally, Fig. 11 depicts the mean effective stress ratio after equalisation (p'_c/p'_0) for the largest initial overconsolidation ratio investigated, so that it can be compared to measurements made in London Clay by Bond & Jardine (1991) around jacked and driven piles. Simulation results agree reasonably well with measured values, both in trend and value.

DISCUSSION

The excess pore water pressure (Δu) was almost consistently underestimated by the simulations which led to an underestimation of the total radial stress. Possible reasons for the discrepancy between the (higher) measured Δu and the (lower) predicted Δu are listed below.

(*a*) The pore pressure is underestimated right after the first step of the numerical simulation, – that is, the strain path method. This was also reported by Whittle *et al.* (1990) who used the strain path method with the MIT-E3 constitutive model. It is therefore likely that one or more assumptions of the strain path method analysis (the lack of cycles, the lack of equilibrium, the constitutive model…) limit its ability to predict excess pore pressures correctly.

(*b*) The outer boundary of the disc shearing model may not extend far enough, which leads to an underestimation of the shear-induced pore pressures.

(*c*) Numerical results simulate a pile driven 100 blows in an undrained manner, the maximum velocity of which exceeds 2 m/s. Field experiments, however, report jacked piles performed at penetration rates ranging from 1 to 100 mm/s, with pauses of a few minutes between the strokes, and under no more than 50 jack strokes. This leads to differences, namely in terms of partial consolidation during installation and in terms of cyclic adaptation of the soil during the shaft–soil shearing cycles. This will be discussed in a future publication.

CONCLUSION

This paper has presented a numerical model aimed at predicting the soil state around the shaft of a driven pile, during and after installation. Installation is modelled as an undrained process which consists of a strain path method simulation (Baligh, 1985), simulating the insertion of the pile toe, followed by a series of shaft–soil shearing events, performed by the disc shearing model (Holeyman, 1985). Equalisation is modelled as a coupled consolidation analysis. The constitutive model used is hypoplasticity for clays (Mašín, 2005). Five initial overconsolidation ratios are investigated and compared to field data gathered in the literature. The numerical model captures some essential features of displacement pile installation in clays, as listed below.

(*a*) During installation, as the pile penetrates further into the ground, stresses vary for a given soil horizon. This is called the h/R effect and is successfully modelled by (i) the stress relief away from the pile toe predicted by the strain path method and (ii) the cycles of shaft–soil shearing imposed by the disc shearing model as blow count increases.

(*b*) At the end of installation, the radial distribution of excess pore pressure exhibits a peak located at a few radii from the pile wall. The pore pressure ratio ($\Delta u/\sigma'_{v0}$) at the pile wall is lower for increasing OCR, whereas the peak $\Delta u/\sigma'_{v0}$, located a few radii away from the pile wall, increases with OCR.

(*c*) At the end of installation, the radial total stress at the pile wall (σ_{ri}) follows a linear trend with OCR in a log–log plot.

(*d*) During equalisation, excess pore pressure (Δu) rises rapidly to a maximum before decreasing to zero. This leads to a short-term minimum in the radial effective stress (σ'_r) at the pile wall.

(*e*) During equalisation, the maximum Δu recorded at the shaft during the short-term increase is linearly increasing with OCR in a log–log plot up to an overconsolidation ratio of approximately 10. For higher overconsolidation ratios, the pore pressure maximum decreases with increasing OCR.

(*f*) At the end of equalisation, the radial effective stress set-up factor is higher than one ($\sigma'_{rc} > \sigma'_{ri}$ at the pile wall) in lightly overconsolidated clay but lower than one ($\sigma'_{rc} < \sigma'_{ri}$ at the pile wall) in overconsolidated clays.

One downside of the model output is the underprediction of the excess pore pressure. This was consistent and most likely stems from an underestimation of the excess pore pressure of the strain path method when it is coupled to the hypoplastic constitutive model.

Nevertheless, the successful predictions of the model can be attributed to five of its characteristics: (*a*) the hypoplastic constitutive model is based on critical state soil mechanics, which leads to a strong dependency on the initial overconsolidation ratio, (*b*) the constitutive model handles cyclic loading, (*c*) the constitutive model is capable of simulating shear-induced dilatancy, (*d*) the strain path method predicts the distortion and reversals of strain associated with the insertion of a pile toe, and (*e*) the disc shearing model produces a cycle of strain under each blow.

ACKNOWLEDGEMENTS

The authors would like to acknowledge Richard Jardine (Imperial College London) and Alain Puech (Fugro GeoConsulting France) for their incisive comments and clear-sighted suggestions about the work presented in this paper.

APPENDIX 1. HYPOPLASTIC, CAM CLAY AND CONVENTIONAL OVERCONSOLIDATION RATIOS

The hypoplastic definition of overconsolidation ratio (OCR*, defined in equation (2)) differs from the overconsolidation ratio used in Cam Clay-based models

$$n_p = \frac{p'_y}{p'} \tag{15}$$

where p'_y is the yield mean effective stress in the v–ln p' plane and p' is the current mean effective stress.

These two definitions of overconsolidation ratio are linked by the following relationship (Muir Wood, 1990)

$$\mathrm{OCR}^* = (n_p)^{\Lambda} \tag{16}$$

where $\Lambda = (\lambda - \kappa)/\lambda$, and λ and κ are the slopes of the normal compression line and the unloading–reloading line, respectively, in the v–ln p' plane.

These definitions all differ from the conventional definition of overconsolidation ratio, relating vertical stresses (in oedometric

conditions) instead of mean stresses

$$\mathrm{OCR} = \frac{\sigma'_{vy}}{\sigma'_v} \tag{17}$$

where σ'_{vy} is the yield vertical effective stress and σ'_v is the current vertical effective stress.

Assuming that the coefficient of earth at rest can be approached by Jâky (1944) and Mayne & Kulhawy (1982) relationships for a normally consolidated and overconsolidated soil, respectively

$$K_{0nc} = 1 - \sin\phi'_{cs} \tag{18}$$

$$K_0 = K_{0nc}\mathrm{OCR}^{\sin\phi'_{cs}} \tag{19}$$

the hypoplastic overconsolidation ratio (OCR*) can be related to the conventional overconsolidation ratio (OCR) though the following relationship

$$\mathrm{OCR}^* = \frac{3}{1+2K_{0nc}}\left(\frac{1+2K_{0nc}}{1+2K_0}\mathrm{OCR}\right)^{\Lambda} \tag{20}$$

Equation (20) is plotted in Fig. 12 for $\phi'_{cs} = 22{\cdot}6°$.

APPENDIX 2. HYPOPLASTIC CONSTITUTIVE MODEL CYCLIC UNDRAINED SIMPLE SHEAR PREDICTION

This appendix summarily depicts the hypoplastic model capabilities by performing a couple of 'one-element' predictions of an undrained simple shear test.

For both simulations, the London Clay parameters described in Table 2 are used. The two initial states are the OCR* = 1·1 and 5 initial states included in Table 3, selected because they are on the wet and dry sides of critical, respectively (Schofield & Wroth, 1968). Both initial states have the same initial void ratio (e_0) so that they have the same shear strength (s_{u0}) of 107·80 kPa.

The shear test is performed as follows: an initial loading of $\gamma_{yx} = 10\%$ is carried out followed by a series of 2·5% shear strain amplitude cycles. The results are depicted in Fig. 13.

Figure 13(a) shows the shear stress during the test. During the initial 10% loading, both samples tend towards the critical state strength, which depends only on ϕ'_{cs} and the initial void ratio – although the latter does not vary during the test (de Chaunac, 2015). The stiffness is much lower for the overconsolidated soil than for the normally consolidated one because the former is at an initial stress five times lower than the latter; the small-strain stiffness (G_0) being given by the following expression (Mašín, 2005)

$$G_0 = \frac{m_R\, p'_0}{r^*\lambda^*} \tag{21}$$

where m_R, r^* and λ^* are model parameters and p'_0 is the initial effective mean stress.

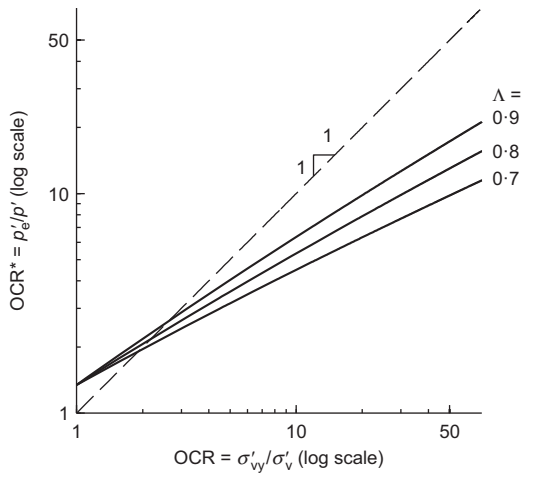

Fig. 12. Conventional overconsolidation ratio (OCR) plotted against hypoplastic overconsolidation ratio (OCR*) for $\phi'_{cs} = 22{\cdot}6°$

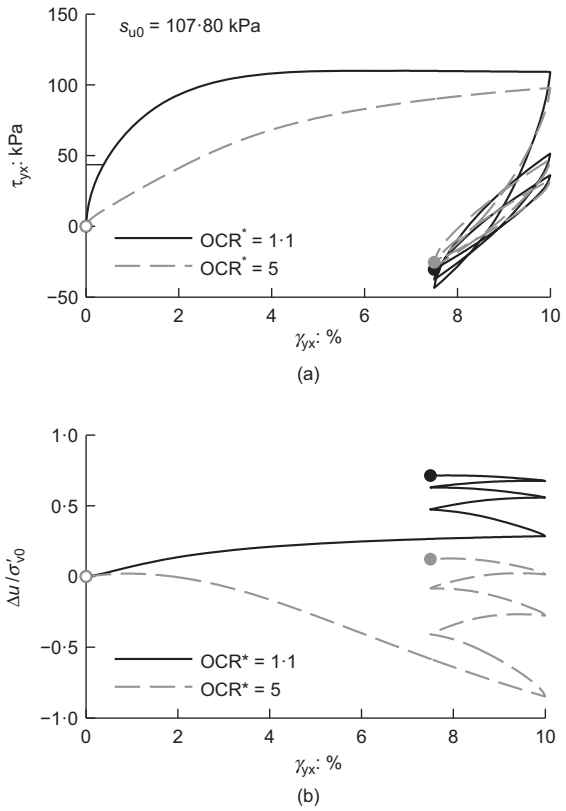

Fig. 13. Predictions of the hypoplastic constitutive model during a cyclic simple shear test: (a) shear stress plotted against shear strain and (b) normalised excess pore pressure plotted against shear strain. The open and shaded data markers correspond to the start and the end of the simulation, respectively

The cyclic loading depicts similar behaviour for both soils, as their states have almost been completely 'swept out of memory' by the 10% initial shearing (Niemunis & Herle, 1997). At each cycle, the soil dissipates energy through hysteretic damping. The shape of each cycle depends on the state (stress, strain and void ratio) and on parameters m_R, R^*, β_r and χ. Parameter m_R controls the small-strain stiffness upon reloading, parameter R^* delimits the size of the 'elastic bubble' and parameters β_r and χ effectively control the amount of hysteretic damping.

The excess pore pressure normalised to the initial vertical effective stress ($\Delta u/\sigma'_{v0}$) is shown in Fig. 13(b). During the 10% initial shearing, the normally consolidated sample exhibits contractancy while the other sample tends towards negative excess pore pressure. The cycles, however, induce a contractant response for both soils. Consequently, the cycles create positive excess pore pressure, the amplitude of which decreases with the number of cycles, as the effective stress decreases.

NOTATION

c_s	soil shear wave velocity
D	pile diameter
e	soil voids ratio
G'	soil shear modulus (effective stress)
G_0	soil small-strain shear modulus
h	height above the pile toe
I	impedance of a dashpot
k	stiffness of a spring
k_r	radial permeability
L_{max}	maximum pile embedment
M	mass
m_R, m_T	stiffness multiplying factors under reverse and perpendicular loading, respectively (hypoplastic model)
N^*	intercept of the isotropic normal compression line at $p' = 1$ kPa in the ln v–ln p' plane (hypoplastic model)

n_p overconsolidation ratio definition according to the critical state theory ($= p'_y/p'$)
p' mean effective stress
p'_e Hvorslev's equivalent mean effective stress – that is the horizontal projection, in the ln v–ln p' plane, of the current stress onto the isotropic normal compression line
R pile radius
R^* size of the small-strain elastic 'bubble' (hypoplastic model)
r radial distance from pile centreline
r^* ratio of shear to bulk modulus (hypoplastic model)
r_b radial extend of the numerical model
S_t sensitivity ($=s_u$[undisturbed]/s_u[remoulded])
s_u undrained shear strength
T dimensionless time used during consolidation ($= k_r\, \sigma'_{v0}\, t/\gamma_w\, R^2$)
t time
U volume rate of the expanding spherical cavity (strain path method)
u pore water pressure
u_z vertical displacement
V velocity of the flow field (strain path method)
v soil specific volume ($= 1 + e$)
v_0 initial velocity of the mass (mass–spring–dashpot system)
v_r, v_z radial and vertical velocity, respectively
z vertical distance from strain path method source
α sprint–dashpot constant
β $= \sqrt{\omega^2 - \alpha^2}$
β_r controls the shape of the stiffness degradation (hypoplastic model)
γ_w unit weight of water
Δu excess pore water pressure
Δu_{max} maximum value of pore water pressure at the pile wall during equalisation
κ slope of the unloading–reloading line in the v–ln p' plane
κ^* initial slope of the unloading–reloading line in the ln v–ln p' plane (hypoplastic model)
Λ $= (\lambda - \kappa)/\lambda$
λ slope of the normal compression line in the v–ln p' plane
λ^* slope of the normal compression line in the ln v–ln p' plane (hypoplastic model)
ρ soil density
ρ_s density of solid phase
ρ_w density of fluid phase
σ_r, σ'_r radial total and radial effective stress, respectively
σ'_v vertical effective stress
τ_f unit skin friction
τ_{rz} shear strain active at the pile/soil interface (negative for a loaded pile)
ϕ'_{cs} critical state friction angle (hypoplastic model)
χ controls the value of the strain at which the soil is swept out of memory (hypoplastic model)
Ψ stream function (strain path method)
ω_n natural frequency of the spring–mass system

Subscripts

0 initial (i.e. in situ) value
c at the end of equalisation
i at the end of pile installation
y at yield

REFERENCES

Andresen, L. & Khoa, H. D. V. (2013). LDFE analysis of installation effects for offshore anchors and foundations. In *Proceedings of the international conference on installation effects in geotechnical engineering* (eds M. A. Hicks, J. Dijkstra, M. Lloret-Cabot and M. Karstunen), pp. 162–168. Leiden, the Netherlands: CRC Press/Balkema.

Azzouz, A. S. & Lutz, D. G. (1986). Shaft behavior of a model pile in plastic empire clays. *J. Geotech. Engng* **112**, No. 4, 389–406.

Azzouz, A. S. & Morrison, M. J. (1988). Field measurements on model pile in two clay deposits. *J. Geotech. Engng* **114**, No. 1, 104–121.

Baligh, M. M. (1985). Strain path method. *J. Geotech. Engng* **111**, No. 9, 1108–1136.

Basu, P., Prezzi, M., Salgado, R. & Chakraborty, T. (2013). Shaft resistance and setup factors for piles jacked in clay. *J. Geotech. Geoenviron. Engng* **140**, No. 3, 04013026.

Bond, A. J. & Jardine, R. J. (1991). Effects of installing displacement piles in a high OCR clay. *Géotechnique* **41**, No. 3, 341–363, http://dx.doi.org/10.1680/geot.1991.41.3.341.

Bottiau, M. (2006). Recent evolutions in deep foundation technologies. In *Proceedings of the DFI/EFFC 10th international conference on piling and deep foundations* (eds J. Lindberg, M. Bottiau and A. F. V. Tol), pp. 46–83. Hawthorne, NJ, USA: Deep Foundations Institute (DFI)

Butterfield, R. (1979). A natural compression law for soils (an advance on e–log p'). *Géotechnique* **29**, No. 4, 469–480, http://dx.doi.org/10.1680/geot.1979.29.4.469.

Butterfield, R. & Bannerjee, P. K. (1970). The effect of pore water pressures on the ultimate bearing capacity of driven piles. *Proceedings of the 2nd southeast Asian conference on soil engineering*, Singapore, pp. 385–394.

Chin, C. T. (1986). *Open-ended pile penetration in saturated clays.* PhD thesis, Massachusetts Institute of Technology, Cambridge, MA, USA.

Chow, F. C. (1996). *Investigations into the behaviour of displacement piles for offshore foundations.* PhD thesis, University of London (Imperial College), London, UK.

Coop, M. R. (1987). *The axial capacity of driven piles in clay.* PhD thesis, Oxford University, Oxford, UK.

Coop, M. R. & Wroth, C. P. (1989). Field studies of an instrumented model pile in clay. *Géotechnique* **39**, No. 4, 679–696, http://dx.doi.org/10.1680/geot.1989.39.4.679.

Coussy, O. (2004). *Poromechanics.* Chichester, UK: John Wiley & Sons, Limited.

de Chaunac, H. (2015). *Numerical investigation of the set-up around the shaft of a driven pile in clay.* PhD thesis, Université catholique de Louvain, Louvain-la-Neuve, Belgium.

de Chaunac, H. & Holeyman, A. (2014). Modelling the behaviour of a disk of clay during pile driving using hypoplasticity. In *EYGEC 2014: Proceedings of the 23rd European young geotechnical engineers conference* (eds M. Arroyo and A. Gens), pp. 33–36. Barcelona, Spain: Universitat Politècnica de Catalunya.

Deeks, A. J. & Randolph, M. F. (1994). Axisymmetric time-domain transmitting boundaries. *J. Engng Mech.* **120**, No. 1, 25–42.

Hamann, T., Qiu, G. & Grabe, J. (2015). Application of a coupled Eulerian–Lagrangian approach on pile installation problems under partially drained conditions. *Comput. Geotech.* **63**, 279–290.

Heerema, E. P. (1980). Predicting pile driveability: Heather as an illustration of the 'friction fatigue' theory. *Ground Engng* **13**, April, 15–20.

Hight, D. W., McMillan, F., Powell, J. J. M., Jardine, R. J. & Allenou, C. P. (2003). Some characteristics of London Clay. In *Proceedings of an international workshop on characterisation and engineering properties of natural soils* (eds T. S. Tan, K. K. Phoon, D. W. Hight and S. Leroueil), vol. 2, pp. 851–908. Lisse, the Netherlands: Balkema.

Holeyman, A. E. (1984). *Contribution à l'étude du comportement dynamique non-lineaire des pieux lors de leur battage.* PhD thesis, Faculté des Sciences Appliquées, Université libre de Bruxelles, Brussels, Belgium (in French).

Holeyman, A. E. (1985). Dynamic non-linear skin friction of piles. *Proceedings of the international symposium on penetrability and drivability of piles*, San Francisco, CA, USA, vol. 1, pp. 173–176.

Jâky, J. (1944). A nyugalmi nyomas tenyezoje (the coefficient of earth pressure at rest). *Magyar Mernok es Epitesz-Eglyet Kozlonye (J. Soc. Hung. Archit. Engrs)* **78**, No. 22, 355–358 (in Hungarian).

Jardine, R., Chow, F., Overy, R. & Standing, J. (2005). *ICP design methods for driven piles in sands and clays.* London, UK: Thomas Thelford.

Jardine, R. J., Standing, J. R. & Chow, F. C. (2006). Some observations of the effects of time on the capacity of piles driven in sand. *Géotechnique* **56**, No. 4, 227–244, http://dx.doi.org/10.1680/geot.2006.56.4.227.

Jassim, I., Coetzee, C. & Vermeer, P. A. (2013). A dynamic material point method for geomechanics. In *Proceedings of the international conference on installation effects in geotechnical engineering* (eds M. A. Hicks, J. Dijkstra, M. Lloret-Cabot and M. Karstunen), pp. 15–23. Leiden, the Netherlands: CRC Press/Balkema.

Karlsrud, K. (2012). *Prediction of load–displacement behaviour and capacity of axially loaded piles in clay based on analyses and interpretation of pile load test results.* PhD thesis, Norwegian University of Science and Technology, Trondheim, Norway.

Karlsrud, K. & Haugen, T. (1985). Axial static capacity of steel model piles in overconsolidated clay. In *Proceedings of the 11th international conference on soil mechanics and foundations engineering*, vol. 3, pp. 1401–1406. Rotterdam, the Netherlands: Balkema.

Konrad, J. M. & Roy, M. (1987). Bearing capacity of friction piles in marine clay. *Géotechnique* **37**, No. 2, 163–175, http://dx.doi.org/10.1680/geot.1987.37.2.163.

Lehane, B. (1992). *Experimental investigations of pile behaviour using instrumented field piles.* PhD thesis, University of London (Imperial College), London, UK.

Lehane, B. M. & Gill, D. R. (2004). Displacement fields induced by penetrometer installation in an artificial soil. *Int. J. Phys. Modelling Geotech.* **4**, No. 1, 25–36.

Lehane, B. M. & Jardine, R. J. (1994a). Displacement-pile behaviour in a soft marine clay. *Can. Geotech. J.* **31**, No. 2, 181–191.

Lehane, B. M. & Jardine, R. J. (1994b). Displacement pile behaviour in glacial clay. *Can. Geotech. J.* **31**, No. 1, 79–90.

Loukidis, D., Salgado, R. & Abou-Jaoude, G. (2008). *Assessment of axially-loaded pile dynamic design methods and review of INDOT axially-loaded pile design procedure*, Technical Report Publication FHWA/IN/JTRP-2008/06. West Lafayette, IN, USA: Indiana Department of Transportation and Purdue University.

Lysmer, J. & Kuhlemeyer, R. L. (1969). Finite dynamic model for infinite media. *J. Engng Mech. Div.* **95**, No. 4, 859–877.

Mašín, D. (2005). A hypoplastic constitutive model for clays. *Int. J. Numer. Analyt. Methods Geomech.* **29**, No. 4, 311–336.

Mašín, D. (2012). *Workshop on hypoplasticity for practical applications.* Stuttgart, Germany: Institute of Geotechnical Engineering, Stuttgart University.

Mayne, P. W. & Kulhawy, F. H. (1982). K_0–OCR relationships in soil. *J. Geotech. Engng* **108**, No. GT6, 851–872.

Muir Wood, D. (1990). *Soil behaviour and critical state soil mechanics.* Cambridge, UK: Cambridge University Press.

Niemunis, A. & Herle, I. (1997). Hypoplastic model for cohesionless soils with elastic strain range. *Mech. Cohesive-frictional Mater.* **2**, No. 4, 279–299.

Pestana, J., Hunt, C. & Bray, J. (2002). Soil deformation and excess pore pressure field around a closed-ended pile. *J. Geotech. Geoenviron. Engng* **128**, No. 1, 1–12.

Poulos, H. G. (1988). *Marine geotechnics.* London, UK: Unwin Hyman Limited.

Randolph, M. F. (2003). Science and empiricism in pile foundation design. *Géotechnique* **53**, No. 10, 847–875, http://dx.doi.org/10.1680/geot.2003.53.10.847.

Randolph, M. & Gourvenec, S. (2011). *Offshore geotechnical engineering*. Milton Park, UK: Spon Press.

Randolph, M. F. & Wroth, C. P. (1979). An analytical solution for the consolidation around a driven pile. *Int. J. Numer. Analyt. Methods Geomech.* **3**, No. 3, 217–229.

Randolph, M. F., Steenfelt, J. S. & Wroth, C. P. (1979). The effect of pile type on design parameters for driven piles. In *Proceedings of the 7th European conference on soil mechanics and foundation engineering*, vol. 2, pp. 107–114. London, UK: British Geotechnical Society.

Rausche, F., Robinson, B. & Likins, G. (2004). On the prediction of long term pile capacity from end-of-driving information. In *Current practices and future trends in deep foundations* (eds J. A. DiMaggio and M. H. Hussein), Geotechnical Special Publication No. 125, pp. 77–95. Reston, VA, USA: American Society of Civil Engineers.

Roy, M., Blanchet, R., Tavenas, F. & La Rochelle, P. (1981). Behaviour of a sensitive clay during pile driving. *Can. Geotech. J.* **18**, No. 1, 67–85.

Sabetamal, H., Nazem, M., Carter, J. & Sloan, S. (2014). Large deformation dynamic analysis of saturated porous media with applications to penetration problems. *Comput. Geotech.* **55**, 117–131.

Sagaseta, C., Whittle, A. J. & Santagata, M. (1997). Deformation analysis of shallow penetration in clay. *Int. J. Numer. Analyt. Methods Geomech.* **21**, No. 10, 687–719.

Schofield, A. & Wroth, P. (1968). *Critical state soil mechanics.* Maidenhead, UK: McGraw-Hill.

Soares, M. M. & Dias, C. R. R. (1989). Behavior of an instrumented pile in the Rio de Janeiro clay. In *Proceedings of the 12th international conference on soil mechanics and foundations engineering*, vol. 1, pp. 319–322. Rotterdam, the Netherlands: Balkema.

Soderberg, L. O. (1962). Consolidation theory applied to foundation pile time effects. *Géotechnique* **12**, No. 3, 217–225, http://dx.doi.org/10.1680/geot.1962.12.3.217.

Steenfelt, J. S., Randolph, M. F. & Wroth, C. P. (1981). Instrumented model piles jacked into clay. In *Proceedings of the 10th international conference on soil mechanics and foundations engineering*, vol. 2, pp. 857–864. Rotterdam, the Netherlands: Balkema.

Su, S. F. (2010). Undrained shear strengths of clay around an advancing cone. *Can. Geotech. J.* **47**, No. 10, 1149–1158.

Tian, Y., Cassidy, M. J., Randolph, M. F., Wang, D. & Gaudin, C. (2014). A simple implementation of RITSS and its application in large deformation analysis. *Comput. Geotech.* **56**, 160–167.

Vanden Berghe, J. F. & & Holeyman, A. (2002). Application of a hypoplastic constitutive law into a vibratory pile driving model. In *Proceedings of the international conference on vibratory pile driving and deep soil compaction (Transvib 2002)* (eds A. Holeyman, J. F. Vanden Berghe and N. Charue), pp. 61–68. Lisse, the Netherlands: Balkema.

Vesić, A. S. (1972). Expansion of cavities in infinite soil mass. *J. Soil Mech. Found. Div.* **98**, No. 3, 265–290.

Vijayvergiya, V. N., Cheng, A. P. & Kolk, H. J. (1977). Effect of soil set up on pile driveability in chalk. *J. Geotech. Engng Div.* **103**, No. 10, 1069–1082.

Whittle, A. J., Aubeny, C. P., Rafalovich, A., Ladd, C. C. & Baligh, M. M. (1990). *Interpretation of in-situ testing of cohesive soils using rational methods*, Technical report. Cambridge, MA, USA: Constructed Facilities Division, Department of Civil Engineering, Massachusetts Institute of Technology.